Proceedings of the ASME 2014 International Mechanical Engineering Congress & Exposition
IMECE2014
November 14-20, 2014, Montreal, Quebec, Canada

IMECE2014-37574

LOW-VELOCITY GLOBAL-LOCAL IMPACT RESPONSE OF SMART COMPOSITE AND SANDWICH COMPOSITE PLATES WITH PIEZOELECTRIC TRANSDUCERS

Theofanis S. Plagianakos
Department of Mechanical Engineering
National Technical University of Athens
Athens, Greece
fanplag@gmail.com

Evangelos G. Papadopoulos
Department of Mechanical Engineering
National Technical University of Athens
Athens, Greece
egpapado@central.ntua.gr

ABSTRACT

Higher-order layerwise piezoelectric laminate mechanics are presented for predicting the low-velocity impact response of pristine composite and sandwich composite plates with piezoelectric transducers. The present formulation enables prediction of the global (temporal variation of impact force, deflection, strain and sensory potential) and local through-thickness (distribution of displacement, stress and strain) impact response of plates with piezoelectric layers or patches. Its enhanced capabilities include efficiency in terms of computational cost, since the system matrices are reduced by means of a Guyan scheme or by using the eigenvectors, thus leading to a plate-impactor system containing a single or two deflection amplitudes per vibration mode, depending on consideration of transverse compressibility. The transfer of the plate-impactor system to state-space enables investigation of the feasibility of real-time active control towards impact force reduction by using output feedback control laws.

INTRODUCTION

Smart sandwich plates with composite faces and foam core, as well as embedded piezoelectric actuators and sensors, combine the superior mechanical properties of sandwich structures, such as, high flexural stiffness to mass ratio, with the capability to monitor the structural response on-site in real-time and to adapt their response according to selected control criteria. At high loading rates, such as in the case of impact loading, damage may occur in the form of matrix cracks and interfacial delaminations, which in cases of low-velocity impact may be invisible. Thus, prediction and monitoring of the global dynamic response and the local through-thickness stress field, is essential in order to keep both design and function within appropriate safety limits. Moreover, the formulation of computationally efficient methodologies for predicting the plate-impactor structural system's response is crucial in order to develop realistic real-time active control algorithms and relevant applications by using the piezoelectric actuators.

Extensive literature reviews on impact on composite structures have been conducted, among others, by Abrate [1], Chai and Zhu [2] and Cantwell and Morton [3]. On the basis of the kinematic assumptions used to predict the response of the impacted structure, the existing models may be divided into two main categories: (i) *mass-spring models* (Shivakumar et al. [4]; Olsson [5]) and (ii) *full continuum models* based on energy equilibrium equations. In both categories, one of the key issues regarding the accuracy of the predicted impact response is the contact law between plate and impactor, which can be Hertzian, elasto-plastic without/with plastic indentation [6], or may take into account damage effects, such as core crushing [7]. Analytical solutions for composite plates subjected to low-velocity impacts have been developed among others by Christoforou and Yigit [8] on the basis of Kirchhoff's plate theory kinematics. Finite element solutions for predicting the low-velocity impact response of composite plates have been reported among others by Sun and Chen [9], who developed a quadratic Lagrange element based on Reissner-Mindlin kinematics and an experimentally determined non-linear indentation. As far as sandwich plates subjected to low-velocity impacts are concerned, higher-order single-layer models have been developed among others by Yang and Qiao [10]. Icardi and Ferrero [11] reported a refined plate element based on global-local 3-D layerwise kinematic assumptions, considered material degradation and predicted damage and through-thickness distributions of transverse displacement and interlaminar shear stress. The idea of embedding piezoelectric sensors to composite structures in order to detect impact location and reconstruct the contact force time-profile was reported in the late 90's by Tracy and Chang [12], and Seydel and Chang [13], and has been elaborated for the design of real-time monitoring networks by Park et al. [14], and Liu and

Chattopadhyay [15]. The active control of impact response of composite plates by means of piezoelectric layers towards the minimization of contact force has been studied by Saravanos and Christoforou [16], who developed an analytical solution based on first-order shear kinematics for the composite laminate and a linear layerwise through-thickness approximation of the electric potential. Yet, the local through-thickness impact response of composite and sandwich composite plates with piezoelectric passive/active transducers in the case of low-velocity impact has not been studied. Moreover, the prediction of the global impact response (impact force, deflection at impact point, electric potential at sensors) is based on the solution of the full plate-impactor system. This approach leads to reduced suitability for real-time control applications due to large matrix sizes and thus increased computational effort.

The objective of the present work is to describe an impact mechanics methodology capable of a computationally efficient prediction of the global and local through-thickness response of pristine composite and sandwich composite plates with piezoelectric actuators and sensors. Moreover, a preliminary study on active control of the force developed during impact of a medium mass impactor on a composite plate is presented.

THEORETICAL FORMULATION

The following paragraphs present the integrated impact mechanics methodology, starting at the general piezoelectric or composite ply level and arriving to the coupled plate-impactor structural system in state-space.

Basic Physical Assumptions

The methodology is based on the following physical assumptions:

- The impact energy is sufficiently low, such as no material damage is induced by the impact event.
- The impact is elastic, thus there is no loss of energy in the form of heat.
- The laminate plies are perfectly bonded together throughout the impact event and subsequent vibration.

Generally, impacts may be categorized to low- and high-velocity ones on the basis of the overall structural response [2]. In the present formulation it is assumed that the impact duration is significantly longer than the travel time of the waves to the boundary, and is enough for the plate to respond [1]. A practical low-velocity threshold has been provided by Cantwell and Morton [3] on the basis of available experimental techniques, as being 10 m/s. The impact velocities studied in the current work are up to 3 m/s.

Governing Material Equations

In general, the laminate layers including the piezoelectric or composite and foam plies are assumed to exhibit linear piezoelectric behaviour. In the following formulation, displacements and electric potential and all other variables arising from these (strains, stresses, etc.) are time-dependent. The ply constitutive equations in the natural coordinate system Oxyz (Fig. 1) have the form:

$$\boldsymbol{\sigma}_i = C_{ij}^E \mathbf{S}_j - \left(e_{mi}\right)^T \mathbf{E}_m$$
$$\mathbf{D}_m = e_{mj}\mathbf{S}_j + \varepsilon_{mm}^S \mathbf{E}_m \quad (1)$$

where i, j=1,…,6 and m=1,…,3; $\boldsymbol{\sigma}_i$ and $\mathbf{S}_j$ are the mechanical stress and engineering strain, respectively, in vectorial notation; $\mathbf{E}_m$ is the electric field vector; $\mathbf{D}_m$ is the electric displacement vector; C_{ij} is the elastic stiffness tensor; e_{mj} is the piezoelectric tensor arising from the piezoelectric charge tensor and the stiffness tensor; and ε_{mm} is the electric permittivity tensor of the material. Superscripts E and S indicate a constant electric field, and strain conditions, respectively. The above equations may encompass the behaviour of both an off-axis homogenized fibrous piezoelectric ply and a passive composite ply (e_{mj}=0). The electric field vector E_m is the gradient of the electric potential $\boldsymbol{\varphi}$ along the natural coordinate system vectors x,y,z:

$$\mathbf{E}_m = -\partial\boldsymbol{\varphi}_m / \partial\mathbf{x}_m \quad (2)$$

In the current work, through-thickness polarized piezoelectric transducers are considered.

Through-Thickness Plate Kinematics

A typical composite or sandwich composite laminate with piezoelectric transducers is subdivided into n discrete layers as shown schematically in Fig. 1.

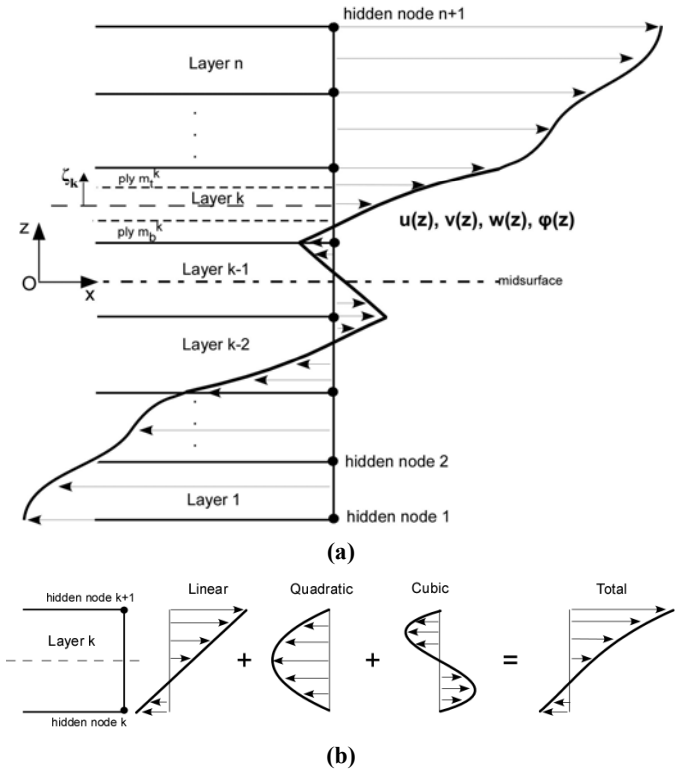

Fig. 1: Typical sandwich piezoelectric composite laminate configuration analyzed with n-discrete layers. **(a)** Discrete layers. **(b)** Assumed displacement and electric potential distribution in each layer.

In the case of composite plates, the displacement field assumed through the thickness of the laminate is based on a 2-D higher-order layerwise formulation (HLPT 2-D), which approximates in-plane displacements and electric potential by piecewise linear, parabolic and cubic functions of the discrete layer thickness, while maintaining displacement continuity across discrete layer boundaries [17]. For the sandwich structures, the core compressibility effects are taken into account by applying a similar through-thickness approximation on the transverse displacement (HLPT 3-D). In this context, the kinematic assumptions take the form:

Both Composite and Sandwich Plates

$$\begin{aligned}
\mathbf{u}^k(x,y,\zeta_k) &= U^k(x,y)\Psi_1^k(\zeta_k) + U^{k+1}(x,y)\Psi_2^k(\zeta_k) \\
&\quad +\alpha_x^k(x,y)\Psi_3^k(\zeta_k) + \lambda_x^k(x,y)\Psi_4^k(\zeta_k) \\
\mathbf{v}^k(x,y,\zeta_k) &= V^k(x,y)\Psi_1^k(\zeta_k) + V^{k+1}(x,y)\Psi_2^k(\zeta_k) \\
&\quad +\alpha_y^k(x,y)\Psi_3^k(\zeta_k) + \lambda_y^k(x,y)\Psi_4^k(\zeta_k) \\
\boldsymbol{\varphi}_z(x,y,\zeta_k) &= \Phi_z^k(x,y)\Psi_1^k(\zeta_k) + \Phi_z^{k+1}(x,y)\Psi_2^k(\zeta_k) \\
&\quad +\alpha_\varphi^k(x,y)\Psi_3^k(\zeta_k) + \lambda_\varphi^k(x,y)\Psi_4^k(\zeta_k)
\end{aligned} \tag{3}$$

Composites Plates (HLPT 2-D)

$$\mathbf{w}^k(x,y,\zeta_k) = w^0(x,y) \tag{4}$$

Sandwich Plates (HLPT 3-D)

$$\begin{aligned}
\mathbf{w}^k(x,y,\zeta_k) &= W^k(x,y)\Psi_1^k(\zeta_k) + W^{k+1}(x,y)\Psi_2^k(\zeta_k) \\
&\quad +\alpha_z^k(x,y)\Psi_3^k(\zeta_k) + \lambda_z^k(x,y)\Psi_4^k(\zeta_k)
\end{aligned} \tag{5}$$

where **u** and **v** are the in-plane displacements, **w** is the transverse displacement, superscripts k=1,…,n denote discrete layer and midsurface, and ζ_k is the local thickness coordinate of layer k defined such that ζ_k=0 at the middle of the discrete layer, ζ_k=1 and ζ_k=-1 at the top and the bottom, of the discrete layer k, respectively. Ψ_1^k, Ψ_2^k are linear and Ψ_3^k, Ψ_4^k are quadratic, cubic interpolation functions, respectively, through the thickness of the layer. U^k, V^k, W^k, U^{k+1}, V^{k+1}, W^{k+1} and Φ_z^k, Φ_z^{k+1} are displacements and electric potential at the bottom and top of the discrete layer k, effectively describing extension and rotation, and electric potential at the terminals, respectively, of the layer, and w^0 is the transverse displacement at the midplane. The terms α_x^k, α_y^k, α_z^k, α_φ^k, λ_x^k, λ_y^k, λ_z^k, λ_φ^k are amplitudes of quadratic (α) and cubic (λ) variations of displacements (subscript x, y and z) and electric potential (subscript φ) through the thickness of the discrete layer. The contributions of these higher-order variations to the in-plane displacement and electric potential distribution through the thickness of the discrete layer vanish at its top and bottom interfaces.

Laminate Energy

The stiffness and mass matrices of the sandwich composite plate are derived on the basis of Hamilton's principle:

$$\int_{t_1}^{t_2}\left(-\int_{A_o}\delta H_L\,dA + \int_{A_o}\delta K_L\,dA + \int_{\Gamma}(\delta\bar{\mathbf{u}})^T\bar{\boldsymbol{\tau}}\,d\Gamma\right)dt = 0 \tag{6}$$

where A_0 denotes the midplane (Fig. 1(a)), $\delta\bar{\mathbf{u}}$ is the vector of all degrees of freedom of the laminate arising from the kinematic assumptions (3)-(5), $\bar{\boldsymbol{\tau}}$ are the tractions at the boundary surface Γ, δH_L and δK_L are the variations of the electromechanical and kinetic energy of the laminate per unit area, expressed as:

$$\delta H_L = \sum_{k=1}^{n}\int_z((\delta\mathbf{S}_i^k)^T\boldsymbol{\sigma}_i - (\delta\mathbf{E}_j^k)^T\mathbf{D}_j)dz \tag{7}$$

$$\delta K_L = \sum_{k=1}^{n}\int_z\frac{1}{2}((\delta\underline{\dot{\mathbf{u}}}^k)^T\rho^k\underline{\dot{\mathbf{u}}}^k)dz \tag{8}$$

where k denotes discrete layer, i=1,…,6 and j=1,2,3, and $\mathbf{S}_i^k, \underline{\mathbf{u}}^k$ are mechanical strain and displacement vectors. Combination of equations (6)-(8) with the strain-displacement relations, the electric field equation (2) and the constitutive equation (1) yields the laminate stiffness, piezoelectric and electric permittivity matrices. In the case of the HLPT 2-D, interlaminar shear stress compatibility is imposed through the thickness of the laminate [17], leading to elimination of 2n+2, higher-order elastic variables. In the case of the HLPT 3-D the out of plane stress compatibility is weakly maintained through the equations of motion (6).

In-Plane Approximation of Elastic-Electric Variables

Before proceeding with integration along the plate's midsurface, as dictated by equation (6), an in-plane approximation of displacements and electric potential of the laminate should be implemented. In the case of a Ritz-type analytical solution, the first order electromechanical variables are approximated by Fourier series expansions, which are expressed in a general form as,

$$\begin{aligned}
W^k(x,y) &= \sum_i^m\sum_j^n \overline{W}_{ij}^k X_{ij}^w(x,y) \\
U^k(x,y) &= \sum_i^m\sum_j^n \overline{U}_{ij}^k X_{ij}^u(x,y) \\
V^k(x,y) &= \sum_i^m\sum_j^n \overline{V}_{ij}^k X_{ij}^v(x,y) \\
\Phi^k(x,y) &= \sum_i^m\sum_j^n \overline{\Phi}_{ij}^k X_{ij}^\phi(x,y)
\end{aligned} \tag{9}$$

where *m*, *n* denote modes along x and y, respectively, and X_{ij} are approximation functions of each variable indicated by superscript, which are derived by satisfying the arbitrary boundary conditions. The higher-order terms of displacement and electric potential are approximated accordingly on the basis of the first-order variable they refer to. The impact load is assumed to act transversely at the impact point and is approximated using the approximation functions of the transverse displacement. The general form of the above approximations includes Navier-type solutions applicable for cross-ply simply-supported plates.

In the case of finite element approximations, the transverse displacement is approximated by implementing either C^1-continuous Hermitian shape functions, as mandated by the explicit imposition of interlaminar shear stress compatibility in HLPT-2D, or C^0-continuous linear Lagrange shape functions in HLPT-3D. The in-plane elastic variables and the electric potential terms are approximated using linear Lagrange shape functions. The finite element solution yields the plate modal matrices, which are reduced and fed into the plate structural subsystem, as explicitly described in the following sections.

Plate Modal Matrices

Substituting the expressions for laminate electromechanical and kinetic energy (7) and (8) into the governing equations of motion (6) and taking into account the strain-displacement relations and the in-plane approximations of displacements and electric potential (9), the plate structural subsystem in discrete form is built for each mode pair *mn*:

$$\begin{bmatrix} \left[\mathrm{M_{uu}}\right]_{mn} & 0 \\ 0 & 0 \end{bmatrix} \begin{Bmatrix} \bar{\ddot{\mathbf{u}}}_{mn} \\ \bar{\ddot{\boldsymbol{\varphi}}}^{\mathrm{P}}_{mn} \end{Bmatrix} + \begin{bmatrix} \left[\mathrm{K_{uu}}\right]_{mn} & \left[\mathrm{K^{PP}_{u\varphi}}\right]_{mn} \\ \left[\mathrm{K^{PP}_{\varphi u}}\right]_{mn} & \left[\mathrm{K^{PP}_{\varphi\varphi}}\right]_{mn} \end{bmatrix} \begin{Bmatrix} \bar{\mathbf{u}}_{mn} \\ \bar{\boldsymbol{\varphi}}^{\mathrm{P}}_{mn} \end{Bmatrix} = \begin{Bmatrix} \mathbf{q}_{mn}(\mathrm{t}) - \left[\mathrm{K^{PA}_{u\varphi}}\right]_{mn} \bar{\boldsymbol{\varphi}}^{\mathrm{A}}_{mn} \\ \mathbf{D}^{\mathrm{P}}_{mn}(\mathrm{t}) - \left[\mathrm{K^{PA}_{\varphi\varphi}}\right]_{mn} \bar{\boldsymbol{\varphi}}^{\mathrm{A}}_{mn} \end{Bmatrix} \tag{10}$$

where superscripts P and A denote passive (sensory) and active piezoelectric layers, and

$$\begin{aligned} \bar{\mathbf{u}}_{mn} &= \left\{ \mathrm{w}^0_{mn}, \mathrm{U}^{\mathrm{k}}_{mn}, \mathrm{V}^{\mathrm{k}}_{mn}, \alpha^{l}_{\mathrm{x}_{mn}}, \alpha^{l}_{\mathrm{y}_{mn}} \right\}^{\mathrm{T}} \\ \bar{\boldsymbol{\varphi}}^{\mathrm{P}}_{mn} &= \left(\left\{ \Phi^{\mathrm{k}}_{\mathrm{z}_{mn}}, \alpha^{l}_{\varphi_{mn}}, \lambda^{l}_{\varphi_{mn}} \right\}^{\mathrm{P}} \right)^{\mathrm{T}} \end{aligned} \tag{11}$$

where k=1,…,n and *l*=1,…,n-1 are the plate modal elastic and electric variable vectors in the case of the HLPT 2-D. Similar vectors are derived in the case of the HLPT 3-D, which additionally contain linear and higher-order terms of transverse displacement, as well as, in-plane higher-order terms eliminated in HLPT 2-D. The vector **q** contains the externally applied loads per unit area, while **D** is the vector of externally applied charges. In the absence of external charge sources, the structural subsystem is condensed as,

$$\left[\mathrm{M_{uu}}\right]_{mn} \bar{\ddot{\mathbf{u}}}_{mn} + \left[\mathrm{K_{cu}}\right]_{mn} \bar{\mathbf{u}}_{mn} = \mathbf{q}_{mn}(\mathrm{t}) + \left[\mathrm{K^{A}_{ce}}\right]_{mn} \bar{\boldsymbol{\varphi}}^{\mathrm{A}}_{mn} \tag{12}$$

where,

$$\left[\mathrm{K_{cu}}\right]_{mn} = \left[\mathrm{K_{uu}}\right]_{mn} - \left[\mathrm{K^{PP}_{u\varphi}}\right]_{mn} \left[\mathrm{K^{PP}_{\varphi\varphi}}\right]^{-1}_{mn} \left[\mathrm{K^{PP}_{u\varphi}}\right]^{\mathrm{T}}_{mn} \tag{13}$$

$$\left[\mathrm{K^{A}_{ce}}\right]_{mn} = \left[\mathrm{K^{PP}_{u\varphi}}\right]_{mn} \left[\mathrm{K^{PP}_{\varphi\varphi}}\right]^{-1}_{mn} \left[\mathrm{K^{PA}_{\varphi\varphi}}\right]_{mn} - \left[\mathrm{K^{PA}_{u\varphi}}\right]_{mn} \tag{14}$$

Reduction of Plate Modal Matrices

As indicated by Eqs. (11) and (12), the size of the mass and stiffness matrices of the plate depend on the through-thickness discretization. For a plate discretized through-thickness by n discrete layers, Eq. (11) yields 4n+1 or 9n+3 independent elastic variables in the case of an HLPT 2-D or HLPT 3-D Ritz-type analytical solution, respectively. These elastic variables determine the size of the mass and stiffness matrix in equation (12). Considering that for predicting the dynamic response of a plate subjected to a point impact the plate-impactor system should be solved for a large amount of mode pairs at each time step, the layerwise through-thickness discretization would lead to mass and stiffness matrices of large size and respective computational cost. In order to reduce this cost and enable implementation of the methodology to real-time control applications, while retaining the information regarding the through-thickness response, appropriate reduction techniques should be applied on the plate subsystem.

Two types of reduction are implemented in the current formulation: (i) A Guyan reduction scheme in the case of Ritz-type Navier solutions and (ii) reduction by means of the modal vectors in the case of other boundary conditions and finite element approximations. The idea behind both reduction techniques is to select a primary (independent) elastic variable and express it as a function of the reduced (dependent) ones. Since the impact force is assumed to act purely in the z-direction (Fig. 1(a)) and thus bending vibration modes are primarily excited, the transverse displacement was selected as the independent variable in both reduction schemes.

In the case of the Guyan reduction applied to the HLPT 2-D Navier solution, the modal vector is related to the transverse displacement as,

$$\bar{\mathbf{u}}_{mn} = \begin{Bmatrix} \mathrm{w}^0_{mn} \\ \mathrm{U}^{\mathrm{k}}_{mn} \\ \mathrm{V}^{\mathrm{k}}_{mn} \\ \alpha^{l}_{\mathrm{x}_{mn}} \\ \alpha^{l}_{\mathrm{y}_{mn}} \end{Bmatrix} = \begin{Bmatrix} \bar{\mathbf{u}}^{\mathrm{i}}_{mn} \\ \bar{\mathbf{u}}^{\mathrm{d}}_{mn} \end{Bmatrix} = \mathbf{T}_{mn} \bar{\mathbf{u}}^{\mathrm{i}}_{mn} = \mathbf{T}_{mn} \mathrm{w}^0_{mn} \tag{15}$$

where $\mathbf{T}_{mn}$ is the modal transformation vector, which arises from consideration of a static load case for independent (superscript i) and dependent (superscript d) elastic variables:

$$\begin{bmatrix} [K_{ii}]_{mn} & [K_{id}]_{mn} \\ [K_{di}]_{mn} & [K_{dd}]_{mn} \end{bmatrix} \begin{Bmatrix} \bar{u}^{i}_{mn} \\ \bar{u}^{d}_{mn} \end{Bmatrix} = \begin{Bmatrix} q^{i}_{mn} \\ 0 \end{Bmatrix} \tag{16}$$

In this context, the plate stiffness matrix for each mode pair *mn* is reduced as:

$$K^{r}_{mn} = \mathbf{T}^{T}_{mn} [K_{cu}]_{mn} \mathbf{T}_{mn} \tag{17}$$

The plate mass matrix is reduced in a similar manner. The plate matrices reduction procedure yields per mode pair *mn* a single term for stiffness and mass, respectively. In the HLPT 3-D Navier solution, the reduction technique is implemented in a similar manner by selecting the top and bottom plate face transverse displacement as independent variables, thus yielding per mode pair *mn* two terms for stiffness and mass, respectively, whereas the rest 9n+1 dependent variables are expressed as a function of top and bottom transverse displacement. A detailed description of the implementation of Guyan reduction technique can be found in [19].

In the cases of other boundary conditions than simple-supports and non cross-ply laminations, the finite element solution is implemented and the reduced modal matrices are derived by multiplication of the plate structural matrices with the modal vectors as,

$$\begin{aligned} [M_{uu}]_{mn} &= \boldsymbol{V}^{T}_{mn} [M] \boldsymbol{V}_{mn} \\ [K_{uu}]_{mn} &= \boldsymbol{V}^{T}_{mn} [K] \boldsymbol{V}_{mn} \end{aligned} \tag{18}$$

The piezoelectric matrices appearing in equations (12)-(14) are reduced in a similar manner.

Both reduction techniques lead to the formulation of the reduced subsystem of the plate, which has the following form:

$$M^{r}_{mn} \ddot{w}^{0}_{mn} + K^{r}_{mn} w^{0}_{mn} = q^{w}_{mn}(t) \tag{19}$$

Plate-Impactor Contact Force

In the present methodology, impactors with hemi-spherical tip are assumed. Linear contact laws are implemented in order to retain low computational cost and facilitate implementation to real-time control applications. In the case of composite plates, the linear elasto-plastic contact law proposed by Yigit and Christoforou [8] is considered. During impact at a point (x_0,y_0), the contact force F_i is assumed to vary linearly with the local indentation, which is defined as the relative distance between the impactor position and the face deflection, which in HLPT 2-D is assumed to be constant through-thickness on the basis of the kinematic assumptions (4):

$$F_i(x_0,y_0) = \begin{cases} k_y \left(w_i - w^0(x_0,y_0) \right) \\ 0 \end{cases} \begin{matrix} , w_i > w^0(x_0,y_0) \\ , w_i \le w^0(x_0,y_0) \end{matrix} \tag{20}$$

where w_i is the vertical distance of the impactor (modelled as a point mass) from the plate's surface position just before impact (Fig. 2) and k_y is the contact stiffness, which depends on impactor radius and elastic properties of impactor and plate material [6]. On the basis of eq. (20), the simulation of a low-energy impact of a steel sphere on a composite plate includes two distinct impact states: (i) aggregation – plate and impactor motion are coupled and (ii) disaggregation – plate and impactor move independently. The trigger for switching between these two distinct states is the relative distance between impactor position and plate midsurface.

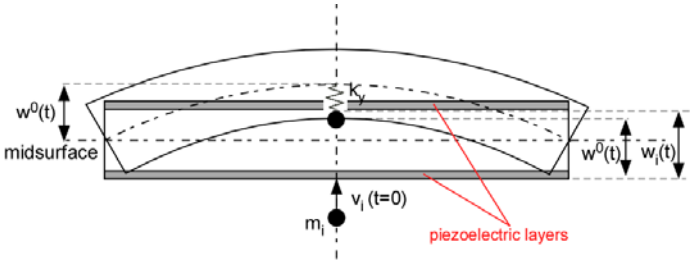

Fig. 2: Schematic representation of the linearized contact model [8] implemented during impact on a composite plate.

In the case of sandwich composite plates, linearized contact laws in the form of equation (20) are adopted, with transverse displacement of the impacted face instead of midplane displacement w^0.

Plate-Impactor Structural System

The plate-impactor structural system is formulated by combining the plate subsystem (19) with the contact force equation (20), the governing equation of motion of the impactor,

$$m_i \ddot{w}_i(t) = -F_i(x_0,y_0,t) \tag{21}$$

and the expression of transverse modal load per unit area q_{mn} by means of Fourier series terms, which in the case of simple supports is,

$$q_{mn}(x_0,y_0) = \frac{4F_i(x_0,y_0)}{L_x L_y} \sin\left(\frac{m\pi}{L_x} x_0\right) \sin\left(\frac{n\pi}{L_y} y_0\right) \tag{22}$$

Thus, the coupled plate-impactor system is formulated in time domain as,

$$[M_s] \begin{Bmatrix} \ddot{w}^{0}_{mn}(t) \\ \ddot{w}_i(t) \end{Bmatrix} + [K_s] \begin{Bmatrix} w^{0}_{mn}(t) \\ w_i(t) \end{Bmatrix} = 0 \tag{23}$$

The above system is finally transferred to state-space in order to facilitate real-time control applications:

$$\begin{aligned} \dot{\underset{\sim}{x}} &= [A] \underset{\sim}{x} + [B] \underset{\sim}{\phi}^{A} \\ \underset{\sim}{y} &= [C] \underset{\sim}{x} \end{aligned} \tag{24}$$

where [A], [B], [C] are the system, input and output matrix, respectively and

$$\underset{\sim}{\mathbf{x}} = \left\{ w^0_{mn}, w_i, \dot{w}^0_{mn}, \dot{w}_i \right\}^T \quad (25)$$

is the vector of state variables. Depending on the case study, the output variables vector $\underset{\sim}{\mathbf{y}}$ may include sensory electric potentials, mechanical displacements, strains and stresses or related time derivatives, such as the electric current density reported in the active control case in the Results section.

RESULTS AND DISCUSSION

In the following paragraphs predictions of the current impact mechanics methodology are compared with Ritz-type analytical solutions for composite plates without/with piezoelectric layers, and the effect of impactor mass on the response is quantified. The global response of composite plates with piezoelectric sensory patches is studied for the case of eccentric impact. The local through-thickness impact response of sandwich composite plates with faces including piezoelectric layers is investigated. Finally, preliminary studies are conducted for actively controlling impact force in composite plates with piezoceramic layers. The electromechanical properties of the materials considered are listed in Table 1.

Table 1: Electromechanical Properties of Materials Considered

Material Properties	Graphite/Epoxy	Foam	PIC 181
Mass Properties			
ρ (kg/m^3)	1578	45	7800
Elastic Properties			
E_{11} (GPa)	120	0.035	84.7
E_{22} (GPa)	7.9	0.035	84.7
E_{33} (GPa)	7.9	0.035	70.4
G_{23} (GPa)	5.5	0.012	27.1
G_{13} (GPa)	5.5	0.012	27.1
G_{12} (GPa)	5.5	0.012	31.9
ν_{12}	0.30	0.40	0.33
ν_{13}	0.30	0.40	0.43
ν_{23}	0.30	0.40	0.43
Piezoelectric Properties			
d_{31} (10^{-12} m/V)	-	-	-120
d_{32} (10^{-12} m/V)	-	-	-120
d_{33} (10^{-12} m/V)	-	-	265
d_{15} (10^{-12} m/V)	-	-	475
d_{24} (10^{-12} m/V)	-	-	475
Dielectric Properties			
ε_{11} (10^{-12} Farad/m)	31	-	13280
ε_{22} (10^{-12} Farad/m)	27	-	13280
ε_{33} (10^{-12} Farad/m)	27	-	10620

Composite Plate with Piezoelectric Transducers

A $[(0/90)_2/0]_S$ Graphite/Epoxy square composite plate was studied as a benchmark case and the effects of boundary conditions, impactor mass and initial velocity were investigated. The plate had edge length of a=0.2 m and thickness aspect ratio of a/h=74, whereas each composite ply had a thickness of 0.135 mm. The present HLPT 2-D formulation is validated with an analytical solution based on first-order shear laminate theory kinematics [16].

As a first validation, the plate was impacted upwards at the centre by a steel sphere having a mass of m_i=8.537 g and an initial velocity at contact v_i=3.0 m/s. The contact stiffness had a value of k_y=6.65e6 N/m [8], as arising from yield strength of a typical Graphite/Epoxy composite material. A single discrete layer was used to model the plate through-thickness and 11x11 bending modes were taken into account for both laminate theories. Fig. 3 shows predicted global impact response for simply-supported (S-S) and clamped-clamped (C-C) boundary conditions. In the former case the plate modal matrices have been derived by a Ritz-type solution, whereas in the latter case by a finite element in-plane approximation. Excellent agreement is observed between predictions of the current methodology and [16], whereas the plate yields a slightly more compliant response than in [16] due to accurate capturing of interlaminar shear effects.

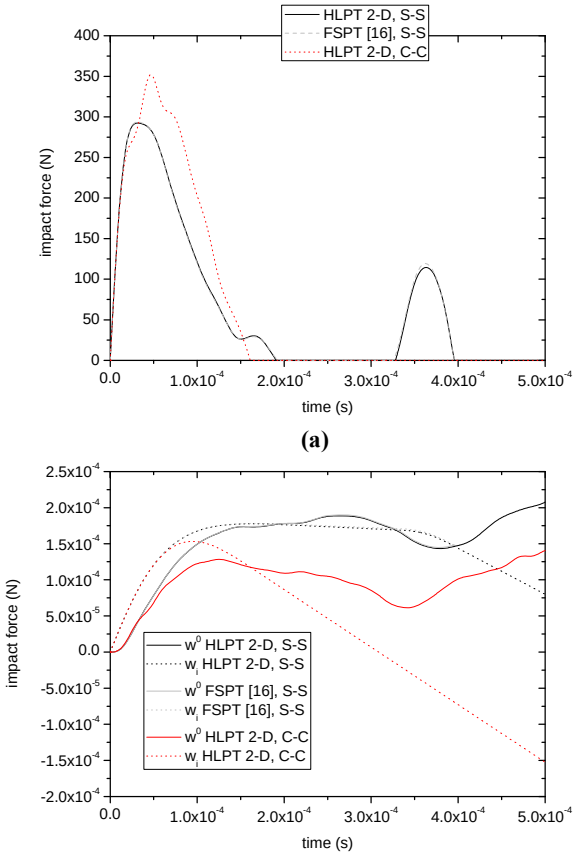

Fig. 3: Validation of current methodology predictions for the case of a small mass impact on a $[(0/90)_2/0]_S$ Gr/Ep plate for two sets of boundary conditions: (a) impact force, (b) plate displacement and impactor position.

However, in the developed method the size of the reduced plate-impactor system was 74x74, whereas the full system, such as in the case of the FSPT, would have a size of 362x362 for equal modes in state space. The required computational

time on a dual core processor (3.06 GHz, 6 MB) for the reduced plate impactor system was 1.5% of that of the full system. In the case of finite element approximations, the system size would depend on the mesh discretization, however it is expected to be far beyond the matrix size in the current method. Overall, the developed method could efficiently capture the wave-controlled impact response of the composite plate (local response occurring prior to reflection of waves from the boundaries, as described in [5]), as well as, the impact chattering observed after t=0.328 ms.

As a second validation, 0.2 mm thick piezoceramic (pzt-4 from Morgan-Matroc Inc. [16]) layers were considered at top and bottom of the simply-supported composite laminate. The plate was modelled using 3 discrete layers through the thickness. A contact stiffness k_y=1.234e7 N/m [16] was implemented. The plate was assumed to be hit upwards at the centre by a spherical impactor of relatively large mass m_i=5.0 kg with initial velocity v_i=1.0 m/sec. Fig. 4(a) shows predicted temporal variation of the impact force using HLPT 2-D, which is in very good agreement with predictions of [16].

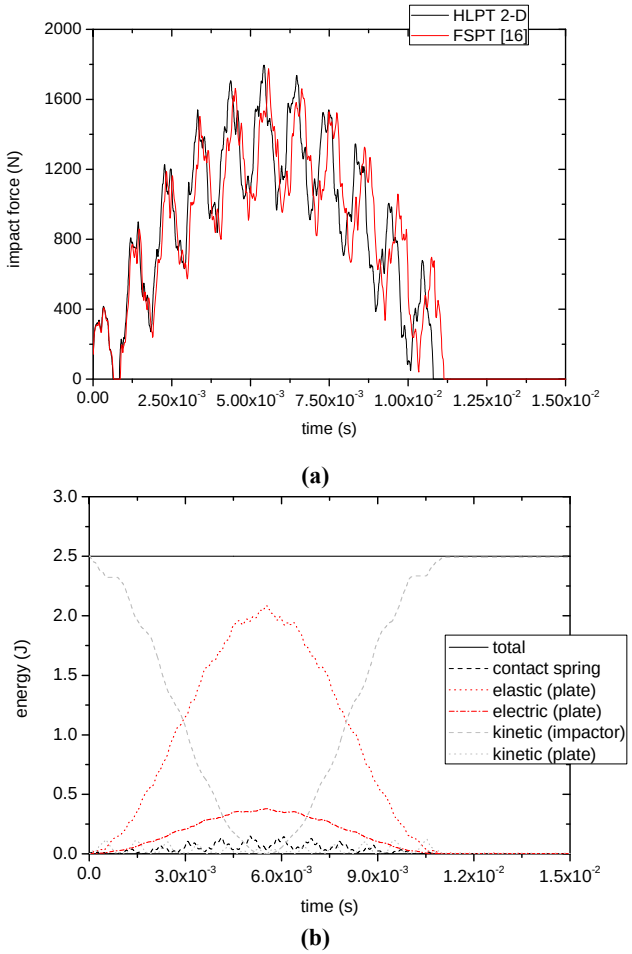

Fig. 4: Validation of current methodology predictions for the case of a 5.0 kg mass impact on a $[\text{pzt-4}/(0/90)_2/0]_S$ plate: (a) impact force, (b) energy equilibrium during impact event.

Due to the large mass of the impactor a "quasi-static" impact response is observed (term defined in [8]), meaning that the response is dominated by the inertia of the impactor, while the plate's vibration is negligible. The validity of the latter comment is illustrated in Fig. 4(b), where the energy equilibrium during impact is shown. As far as computational effort is concerned, the developed method leads to a plate-impactor system of size 74x74 in state space, as in the previous case study, and to similar computational gain, whereas the solution of a full system of size 938x938 would have been required in the case of no reduction.

The attachment of piezoelectric patches on the plate faces is a more practical configuration towards realistic applications. Moreover, impact does generally not occur at the centre of the plate. Thus, the impact response of the simply-supported plate was additionally studied for an impact of a spherical impactor of mass m_i= 0.1 kg and initial velocity v_i=1 m/s at point x_0(a/8,a/8) in the case that four piezoceramic patches with dimension 10x10x0.25 mm are symmetrically attached on each plate face (Fig. 5).

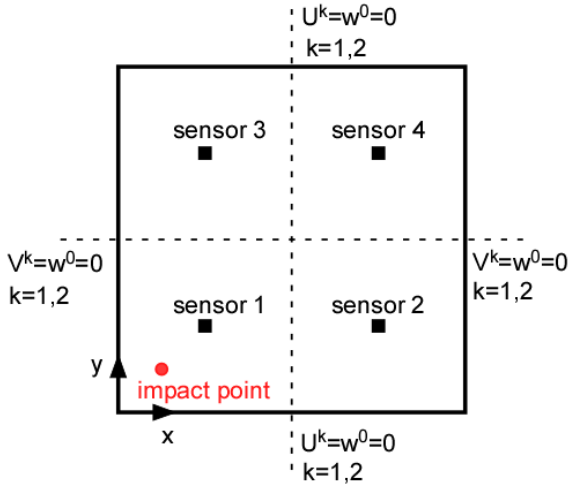

Fig. 5: Simply-supported composite plate with piezoelectric patches. Applied boundary conditions are reported at the plate edges.

The inclusion of the patches does practically not affect the plate's dynamic response in terms of modal frequencies, stiffness and mass, thus they were not modelled and the electric potential (sensory signal) was predicted at the central point of the patch without being averaged, by means of the mechanical strains and the second constitutive equation (1). Predicted transverse displacement at the impact point and in the centre of the patches are presented in Fig. 6(a). It is interesting that during aggregation between plate and impactor the transverse displacement near the impact point exceeds the deflection predicted at the impact location. As expected, the signal of the sensor being nearest to the impact location is initially higher than the signals of the other sensors, as shown in Fig. 6(b).

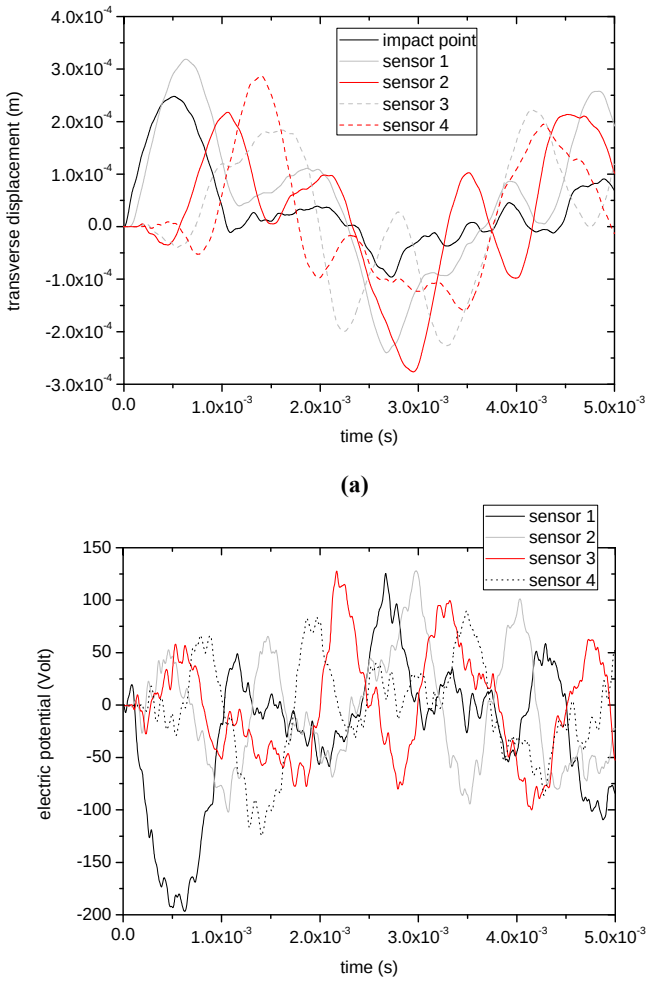

Fig. 6: Impact response of an eccentrically hit $[(0/90)_2/0]_S$ Gr/Ep plate with piezoceramic patches: (a) transverse displacement, (b) sensory signals at the impacted face patches.

Sandwich Composite Plate with Piezoelectric Layers

The impact response of a square $[PIC\ 181/0/foam]_s$ sandwich composite plate of thickness aspect ratio a/h = 31 was studied. The plate consisted of two surface attached piezoelectric layers, each having a thickness of 0.2 mm, Graphite/Epoxy faces of 2 mm each and a 15 mm PVC foam. The plate was impacted upwards at the centre of the bottom face by a mass of m_i = 0.25 kg having an initial velocity of 1 m/s. A contact stiffness k_y=1.234e7 N/m [16] was assumed. The HLPT 3-D formulation was used for predicting the global/local impact response of the plate.

The plate was modelled using five discrete layers through-thickness, namely one for each material sublaminate, resulting to 46 deflection-dependent DOF per mode and a reduced structural system of size 258x258 in state-space for 15x15 modes, whereas solution of a system of size 6146x6146 would be required in the case of a full structural system of an unreduced corresponding analytical solution. Fig. 7 shows the predicted global impact response of the plate.

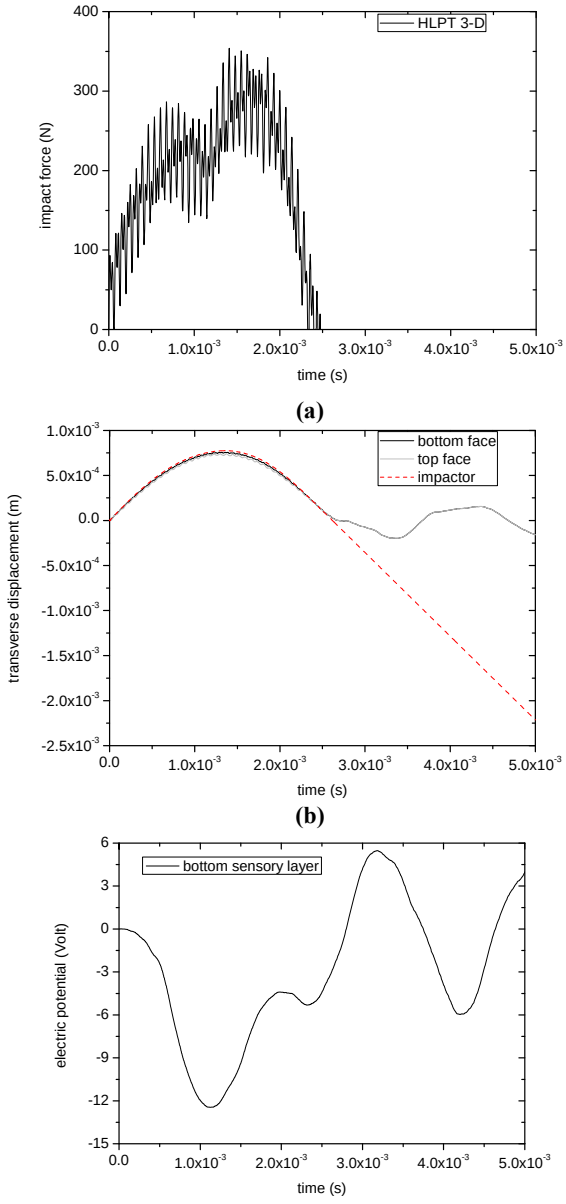

Fig. 7: Global impact response of a sandwich composite plate with piezoceramic layers: (a) impact force, (b) transverse displacement, (c) electric potential at sensory layers.

In Fig. 8 the local through-thickness stress response is presented, at points of maximum values at the timestep corresponding to maximum impact force. The predicted stress distributions reveal the benefit of implementing higher-order layerwise kinematic assumptions, since piecewise through-thickness variations up to second order can be efficiently captured using a minimum number of discrete layers. The latter is a major advantage compared to linear layerwise laminate theories, which would require a large number of discrete layers and thus degrees of freedom in order to capture such through-thickness stress profiles. On the other hand, the lack of explicit imposition of shear stress compatibility equations in the case of

the HLPT 3-D leads to non-zero interlaminar shear stresses at the free faces, although they tend to get to zero.

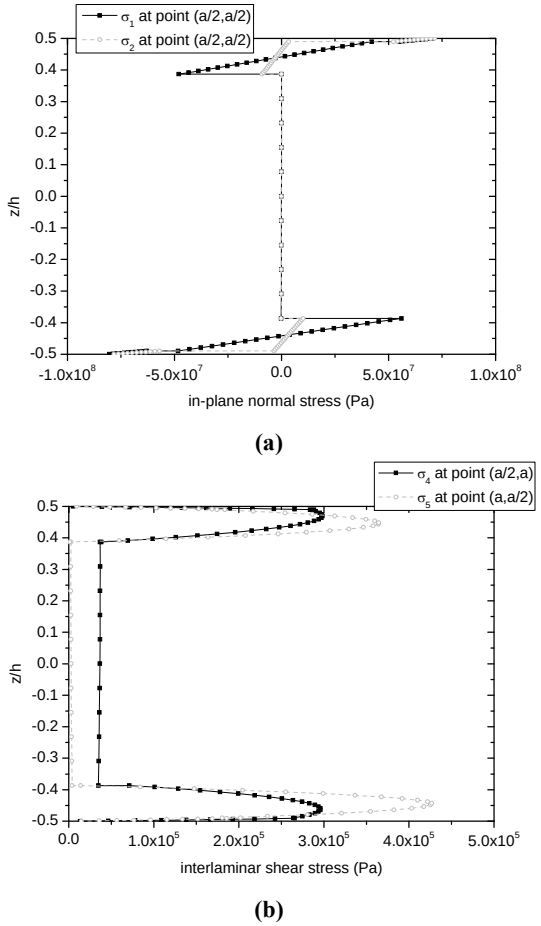

Fig. 8: Local through-thickness impact response of a sandwich composite plate with piezoceramic layers: (a) in-plane stress, (b) interlaminar shear stress.

Preliminary study on Active Control

A preliminary feasibility study was conducted regarding the active control of the impact response of a $[(0/90)_2/0/(0/90)_2/p^P/p^A]$ composite plate towards impact force reduction. Two piezoelectric layers were assumed to be attached to the bottom face of the composite plate studied above. Their interface was grounded and the 0.25 mm thick outer layer was configured to act as an actuator, whereas the 0.125 mm thick inner layer provided the sensory signals.

The output of the state-space system of equation (24) was assumed to be the electric current density (current per unit area), meaning that it would be possible to measure the electric current flow through practically short-circuited piezoelectric terminals of the sensory layer. The plate was impacted at its centre by an impactor having a mass of m_i=0.5 kg and an initial velocity v_i=1 m/s, and 3x3 bending vibration modes were taken into account. The impact solution was programmed in Simulink in order to facilitate realization of active control in a planned experimental configuration. A proportional (P) output feedback control law with gain k_p=10 was implemented, whereas the desired output value was zero, meaning that no current should flow through the piezoelectric sensor terminals. Fig. 9 illustrates the passive (open-loop) and active (closed-loop) global response. The current impact case yields impact chattering and maximum force after the first aggregation between plate and impactor. By means of the active control, the force is reduced and the motion of plate and impactor becomes smoother. It should be noted that the realistic applicability of the current control attempt is still under consideration and will be proved by means of measurements, planned to be conducted in an experimental configuration developed at the CSL Lab (Fig. 10).

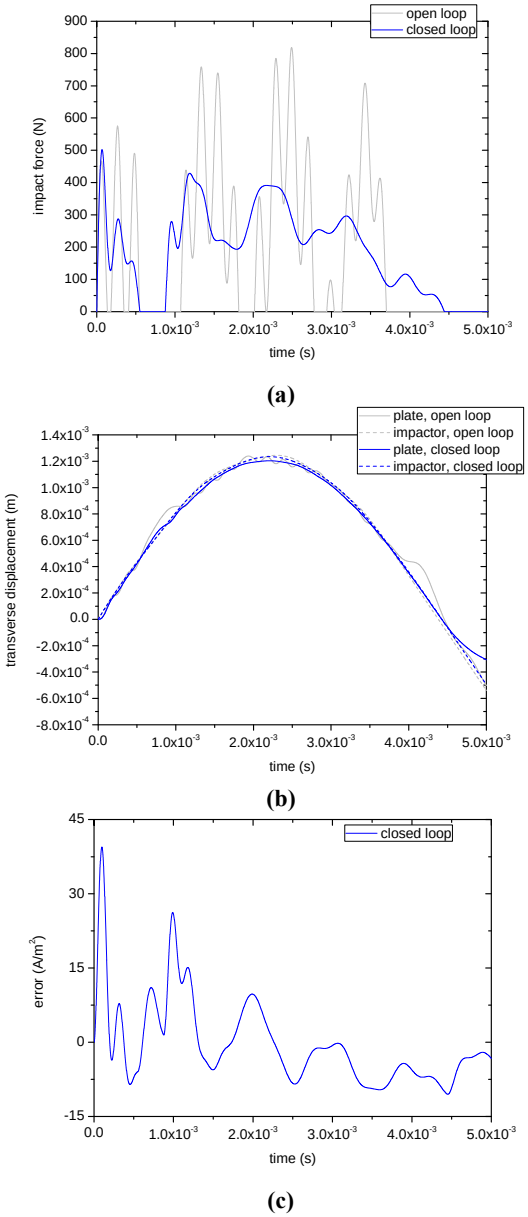

Fig. 9: Active control of impact force in a composite plate with piezoceramic layers: (a) impact force, (b) transverse displacement, (c) error to desired value of electric current density.

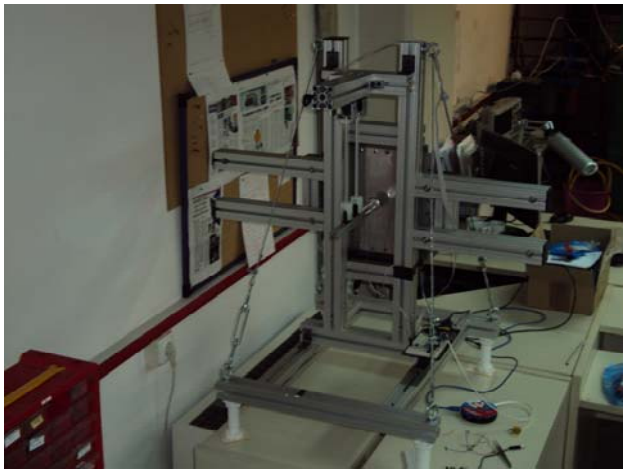

Fig. 10: Experimental configuration for impact testing.

SUMMARY

The present integrated higher-order layerwise mechanics methodology enables prediction of the coupled electro-mechanical impact response of composite and sandwich composite plates with piezoelectric transducers. Its major advantage lies in its computational efficiency, as it leads to a plate-impactor system of minimum size, whereas it may accurately capture the local through-thickness response on the basis of its sophisticated kinematics. A preliminary study on the feasibility of active reduction of impact force was conducted; however, the controller applicability must be experimentally tested. This will be the subject of subsequent work.

ACKNOWLEDGMENTS

The research leading to the results presented in this work has received funding from the People Programme (Marie Curie Actions) of the European Unions' Seventh Framework Programme (FP7/2007-2013) under REA grant agreement n^{o} 299089.

REFERENCES

[1] Abrate, S., 1997, "Localized Impact on Sandwich Structures with Laminated Facings," ASME Appl. Mech Rev., 50(2), pp. 69-82.

[2] Chai, G. B., and Zhu, S., 2011, "A Review of Low-Velocity Impact on Sandwich Structures," J. Mater. Des. Appl., 225, pp. 207-230.

[3] Cantwell, W. J., and Morton, J., 1991. "The impact resistance of composite materials – a review," Composites, 22(5), 135-142.

[4] Shivakumar, K. N., Elber W., and Illg, W., 1985, "Prediction of Impact Force and Duration due to Low-Velocity Impact on Circular Composite Laminates," ASME J. Appl. Mech., 52(3), pp. 674-680.

[5] Olsson, R., 2003, "Closed Form Prediction of Peak Load and Delamination Onset under Small Mass Impact," Comp. Struct. 59(3), 341-349.

[6] Christoforou, A. P., Yigit, A. S., and Majeed, M., 2013, "Low-Velocity Impact Response of Structures with Local Plastic Deformation: Characterization and Scaling," ASME J. Comput. Nonlin. Dyn., 8(1), pp. 011012-1-011012-10.

[7] Olsson, R., and McManus, H. L., 1996, "Improved Theory for Contact Indentation of Sandwich Panels," AIAA J., 34(6), pp. 1238-1244.

[8] Christoforou, A. P., Yigit, A. S., 1998, "Characterization of Impact in Composite Plates," Comp. Struct., 43(1), pp. 15-24.

[9] Sun, C. T., and Chen, J. K., 1985, "On the Impact of Initially Stressed Composite Laminates," J. Comp. Mater., 19(6), pp. 490-504.

[10] Yang, M., and Qiao, P., 2005, "Higher-Order Impact Modelling of Sandwich Structures with Flexible Core," Int. J. Solids Struct., 42(20), pp. 5460-5490.

[11] Icardi, U., and Ferrero, L., 2009, "Impact Analysis of Sandwich Composites Based on a Refined Plate Element with Strain Energy Updating," Comp. Struct., 89(1), pp. 35-51.

[12] Tracy, M., and Chang, F. K., 1998, "Identifying Impacts in Composite Plates with Piezoelectric Strain Sensors, Part I: Theory," J. Intel. Mat. Syst. Str., 9(11), pp. 920-928.

[13] Seydel, R, and Chang, F. K., 2001, "Impact Identification of Stiffened Composite Panels: I. System Development," Smart Mater. Struct., 10(2), pp. 354-369.

[14] Park, J., Ha, S., and Chang, F. K., 2009, "Monitoring Impact Events Using a System-Identification Method," AIAA J., 47(9), pp. 2011-2021.

[15] Liu, Y., and Chattopadhyay, A., 2013, "Low-Velocity Impact Damage Monitoring of a Sandwich Composite Wing," J. Intel. Mat. Syst. Str., 24(17), pp. 2074-2083.

[16] Saravanos, D. A., and Christoforou, A.P., 2002, "Impact Response of Adaptive Piezoelectric Laminated Plates," AIAA J., 40(10), pp. 2087-2095.

[17] Plagianakos, T. S., and Saravanos, D. A., 2008. "Coupled High-Order Layerwise Laminate Theory for Sandwich Composite Plates with Piezoelectric Actuators and Sensors," Proc. 19th International Conference on Adaptive Structures Technologies (ICAST), Ascona CH.

[18] Dugundji, J., 1988, "Simple Expressions for Higher Vibration Modes of Uniform Euler Beams," AIAA J., 26(8), pp. 1013-1014.

[19] Plagianakos, T. S., and Papadopoulos E. G., 2014, "Low-Energy Impact Response of Composite and Sandwich Composite Plates with Piezoelectric Sensory Layers," Int. J. Solids Struct., 51(14), pp. 2713-2727.